Title
Monitoring the Coastal Water Quality of Santa Monica Bay Area, Los Angeles, California Using Sentinel-2

Author
Kong, Yuwei

Publication Date
2021

Peer reviewed|Thesis/dissertation

UNIVERSITY OF CALIFORNIA

Los Angeles

Monitoring the Coastal Water Quality of Santa Monica Bay Area, Los Angeles, California Using Sentinel-2

A thesis submitted in partial satisfaction

of the requirements for the degree Master of Science

in Civil Engineering

by

Yuwei Kong

2021

ABSTRACT OF THE THESIS

Monitoring the Coastal Water Quality of

Santa Monica Bay Area, Los Angeles, California Using Sentinel-2

by

Yuwei Kong

Master of Science in Civil Engineering

University of California, Los Angeles, 2021

Professor Jennifer Ayla Jay, Chair

The application of remotely sensed data to water quality monitoring is an active area of research nowadays, as GIS and remote sensing can reduce the cost and enlarge the scale of ground observation. However, a major challenge is the calibration of satellite-derived data with *in situ* data, which are sometimes difficult and expensive to acquire compared with remote sensing data. This study aims to investigate the effectiveness of Sentinel-2 for estimating coastal water quality in the Santa Monica Bay (SMB), California. Surface reflectance values are obtained from the Copernicus Sentinel-2 and remote sensing derived turbidity values are calculated by ACOLITE. *In situ* total suspended solids (TSS), absorbance, light transmission, and fecal indicator

bacteria (FIB) have been tested to compare with the satellite data. The results of regression analysis demonstrate that remote sensing can offer preliminary qualitative estimates of coastal water quality in the SMB area.

TABLE OF CONTENTS

Acknowledgments

I would like to express my gratitude to my advisor, Dr. Jennifer Jay, for her continued support and encouragement. I would like to thank the following people for helping me finalize the project: Marisol Cira Hernandez, Ileana Callejas and Wayne Hung. I wish to express my special thanks to LA sanitation providing the unpublished data. I'm grateful to all of my friends and family for their understanding and support.

1. Introduction

Accurate and timely remote observation of coastal water quality and its ensuing environmental changes in biogeochemistry is of great importance for a wide variety of nearshore cities (Ouellette & Getinet, 2016; M. J. McCarthy et al., 2017). Turbidity is an optically active water quality parameter related to the presence of suspended particles in water bodies – the larger the concentration of suspended particles, the higher the turbidity (Ritchie, 1976; Chawla et al., 2020). It affects the attenuation of light in water, thereby increasing water opacity, which directly hinders aquatic life by influencing photosynthetic activities (Cloern, 1987; Bilotta & Brazier, 2008; Güttler et al., 2013; Sebastiá-Frasquet et al., 2019). Turbidity is impacted by weather, climate patterns, and human activities along the coasts (M. J. McCarthy et al., 2017; Luis et al., 2019). Thus, understanding the large-scale spatiotemporal dynamics of turbidity is crucial to coastal environment management and protection.

Coastal water of the Santa Monica Bay (SMB) area is an ecologically important marine habitat as well as part of the iconic famed Southern California beaches for tourists and visitors. However, according to the 2020 annual California Beach Report Card released by Heal the Bay, four out of the top ten "Beach Bummers" – the most bacteria-laden beaches – are in Southern California. One of those beaches - Marina del Rey Mother's Beach, located in the SMB area, came in at No. 5 on the list (Ginger et al., 2021). With over 12 million people living in the bordering coastal counties, millions of gallons of domestic, commercial, and industrial wastewater are generated and treated daily by the surrounding wastewater treatment plants, and then released directly to the

coastal water of the SMB (Gierach et al., 2017; U.S. Census Bureau, 2021). That necessitates continuous observation of coastal waters around that area to guarantee that water quality meets human health standards. Coastal water monitoring has historically relied on *in situ* measurements, which are time consuming, expensive and labor intensive (Glasgow et al., 2004; Akbar et al., 2010). Besides, field observations are spatially and temporally limited due to high associated coasts and sparse sampling stations and hence may overlook the associated aquatic responses and transport related to change of water quality (Gierach et al., 2017).

Remote sensing techniques are a highly effective way of regarding the state of the oceans and coasts due to the limits in ground-based observations. Mapping of water quality of coastal waters using remote sensing has been carried out since 1970s (Garg et al., 2020), with the launch of first ocean color sensor, Coastal Zone Color Scanner (Gordon et al., 1980; Hovis et al., 1980). Photons pass through the atmosphere and reach the sea surface, where they will be either scattered or absorbed based on the water surface condition (Büttner et al., 1987). Their spectral responses to these various surface conditions are detected by ocean color sensors and recorded in a satellite image. Satellite observation provides continuous and reasonably accurate data over a complete geographic area of water body on a synoptic scale. Plenty of work have been done on this topic, illustrating that using satellite data for water quality monitoring is feasible. However, it is still difficult to monitor coastal water turbidity due to optical complexity of coastal waters and imprecise atmospheric correction of imagery. Most of the research have been done focusing on the inland water bodies (Table 1).

Many Multispectral Remote Sensing studies of optically active water quality parameter retrieval have been conducted using specially designed ocean color sensor with a large spatial resolution, such as the Coastal Zone Color Scanner (CZCS) with a 825 m resolution (Hoge et al., 1995), the Along Track Scanning Radiometer (ATSR) with a 1000 m resolution (Donlon & Robinson, 1998), the Sea-viewing Wide Field of view Sensor (SeaWIFS) with a 1130 m resolution (Kahru & Mitchell, 2001), the Moderate-resolution Imaging Spectroradiometer (MODIS) with a 250-1000 m resolution (Nezlin et al., 2007), and the Visible Infrared Imaging Radiometer Suite (VIIRS) with a 375-750 m resolution (Cao et al., 2013). Typically, these sensors have high temporal resolution, making them more suitable for continuous monitoring but resulting in coarse spatial resolution or low spectral resolution. No sensor could have a high spectral, spatial, and temporal resolution at the same time: there is a compromise needed between types of resolution (Hellweger et al., 2004; Nazeer & Nichol, 2016). Sensors with high temporal resolution are ideal for homogeneous areas of open ocean but can hardly resolve the near shore environment of a spatially complicated coastal area. Hence, compared with current multi-spectral missions, Sentinel-2 Multispectral Instrument (MSI) provides an unprecedented combination of capabilities with both high temporal and spatial resolution by double satellites orbit. It offers the longevity of successive missions with the possibility to resolve complex and small-scale features over nearshore regions.

This study aims to validate the ability of Sentinel-2 data for estimating water quality around the coastal areas in the Santa Monica Bay. We first analyzed the existing

field data (light transmission) from 2018 to 2019 provided by LA Sanitation to compare with the Sentinel-2 derived turbidity. To further verify the results, we collected coastal water samples from summer 2021 to fall 2021, and specifically focused on the optically active water quality indicator, absorbance. Other *in situ* parameters including fecal indicator bacteria (FIB) and total suspended solids (TSS) are also compared in our study as a supplementary validation.

Table 1. Historical ocean-color sensors used to remotely assess and monitor water qualities.

Water bodies	Sensor	Water quality index	Performance (R^2)	Study area	Reference
Inland	HICO	Chlorophyll-a	0.940	Yangtze River	(Shanmugam et al., 2018)
	AISA	Turbidity	0.937	Casey Lake and Sliver Lake	Sugumaran, 2007
		Secchi Disk Depth	0.855		
		Chlorophyll-a	0.891		
	ALI	Colored Dissolved Organic Matter	0.830	Finland and Sweden lakes	Kutser et al., 2005
	Hyperion	Chlorophyll-a	0.707	Lake Atitlan	Flores-Anderson et al., 2020
	MODIS	Total Suspended Solids	0.859	Apalachicola Bay	S. Chen et al., 2011
Coastal	Landsat 8 OLI	Chlorophyll-a	0.890	Santa Monica Bay	Trinh et al., 2017
	Landsat 8	Phosphates	0.955	Playa Colorada Bay	González-Márquez et al., 2018

2. Study Area

Los Angeles (latitude/ longitude 34°03′N 118°15′W), with a population of 3.8 million in 2020, is the second largest city in the United States and the largest city in California (U.S. Census Bureau, 2021). It lies in a basin in the Los Angeles basin in Southern California, adjacent to the Pacific Ocean, with a Mediterranean climate (Peel et al., 2007). The average annual precipitation in Los Angeles is 379 mm, mainly occurring from November through March, mostly as moderate rain showers but also as heavy rainfall during winter storms. Rainfall is generally higher in the hills and coastal slopes of the mountains due to the orographic uplift (Bray et al., 1999). There is not much rain in summer days. The semi-permanent high pressure area of the north Pacific Ocean is a dominating factor in the weather of Los Angeles. This pressure center moves northward in summer, holding storm tracks well to the north, and consequently, the coastal area of LA receives little or no precipitation from this source during that period. In winter, the Pacific high moves southward, allowing storm centers to swing into and across the coast (*Climate of Los Angeles, California*, 2000). Los Angeles has about 75 miles of coastline from Malibu to Long Beach. It has a wide range of beach environments, from flat, nondescript stretches of sand to scenic coves, rugged bluffs, and rocky tide pools.

The study area, the coastal waters of Santa Monica Bay, falls within the West Los Angeles area. Its marine environment is directly affected by the densely populated Los Angeles area. The large urban population produces tons of wastewater from different sources, which is treated daily by various local wastewater treatment facilities and

discharged directly into the coastal waters of the Santa Monica Bay. Except for being the most popular coastal area in the United States, the Santa Monica Bay is also considered a heavily polluted coastline area nationwide. Thus, water quality monitoring for this area is more frequent and stricter compared with other areas.

Figure 1. Map of study area and *in situ* light transmission sampling sites

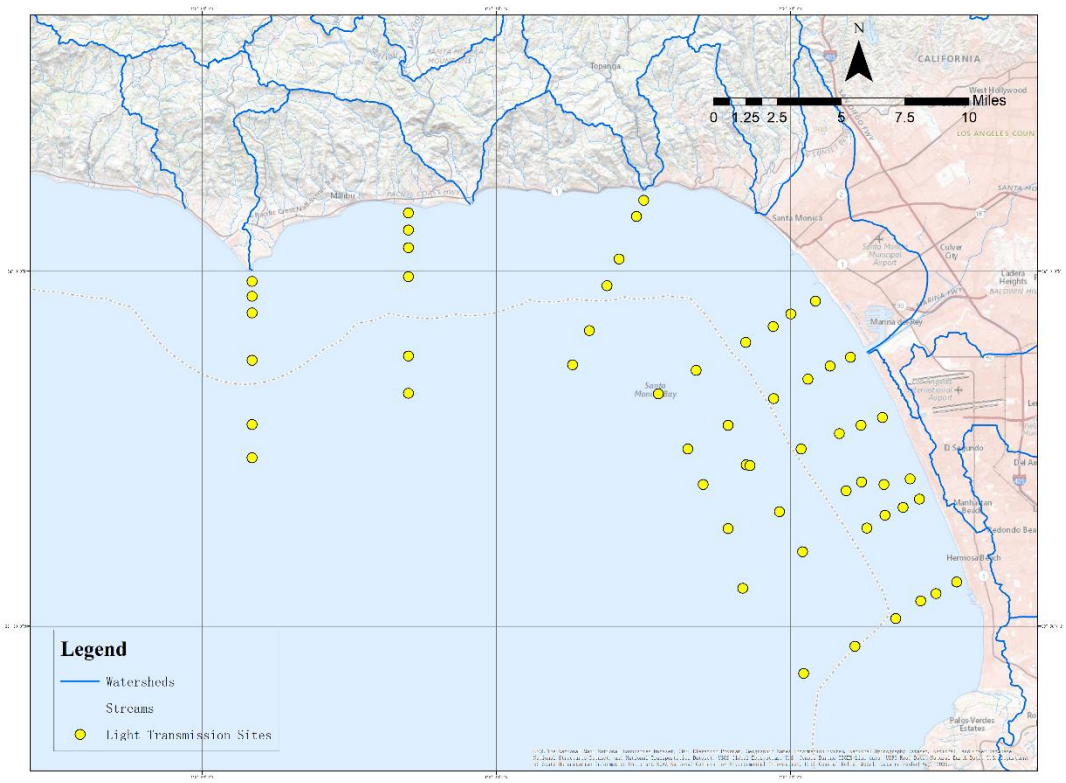

3. Materials and Methods

3.1 Satellite remote sensing data

3.1.1 Satellite Image Acquisition

As part of the European Space Agency (ESA) Copernicus Earth Environment Monitoring Program, SENTINEL-2 is a high-resolution, wide-swath, multi-spectral imaging mission composing of two polar-orbiting satellites: Sentinel-2A and Sentinel-2B, which were launched on June 23rd 2015 and March 7th 2017, respectively. The program provides accurate, timely and easily accessible information to improve the management of the environment, understand and mitigate the effects of climate change. Both satellites are carried with a Multispectral Instrument with 13 spectral bands, ranging from the visible and near-infrared (NIR) to the shortwave infrared to help monitoring vegetation, soil, water cover, and inland waterways and coastal areas. The MSI for Sentinel-2 satellites has different spatial resolutions depending on the spectral bands: four visible and NIR bands at 10 meters, six red edge and shortwave infrared bands at 20 meters and three clouds screening/ atmospheric correction bands at 60 meters (Table 2). The swath of Sentinel-2 images is 290 km, with a five-day revisit time for our study area. Hence, Sentinel-2 is well suited as a data source for water quality observations.

The Sentinel-2 data were downloaded from the United States Geological Survey (USGS) EarthExplorer (https://earthexplorer.usgs.gov/) after filtering the images with cloud coverage ≤ 70%. We used the Level-1C (T11SLT) tile top-of-atmosphere

(TOA) reflectance Sentinel-2A/B data for this study, which including radiometric and geometric corrections, to maintain the uniformity of atmospheric correction.

Table 2. Bandwidths of the Sentinal-2 Multispectral Instrument (MSI) sensor

Band Number	Central Wavelength (nm)	Bandwidth (nm)	Spatial Resolution (m)
1	443	20	60
2	490	65	10
3	560	35	10
4	665	30	10
5	705	15	20
6	740	15	20
7	783	20	20
8	842	115	10
8a	865	20	20
9	945	20	60
10	1375	30	60
11	1610	90	20
12	2190	180	20

3.1.2 Atmospheric Correction Methodologies

The ACOLITE software (https://odnature.naturalsciences.be/remsem/software-and-data/acolite, version 20210114.0) developed at Royal Belgian Institute of Natural Sciences (RBINS) for aquatic applications was used for atmospheric correction (AC). The processor outputs several parameters derived from water reflectance and can generate RGB composites and PNG maps as well (Vanhellemont & Ruddick, 2014, 2015, 2016).

There are two algorithms for AC available in ACOLITE, the default “Dark

Spectrum Fitting (DSF)" algorithm (Vanhellemont & Ruddick, 2018; Vanhellemont, 2019, 2020) and the older "Exponential extrapolation (EXP)" algorithm (Vanhellemont & Ruddick, 2014, 2015, 2016). We used the DSF algorithm for this study. This algorithm works better for meter-scale (MR) optical satellite imagery, by estimating the atmospheric path reflectance based on multiple targets found in the images (typically water pixels and ground-level object shadows), which are selected according to the lowest observed top-of-atmosphere reflectances in all bands. The best band is selected automatically, which could avoid unrealistic negative reflectances after the AC (Vanhellemont & Ruddick, 2018).

3.1.3 Data Processing

The Sentinel-2A/B images were processed in ACOLITE to derive turbidity in Formazine Nephelometric Units (FNU), by using the Dogliotti et al. (2015) algorithm showing below:

$$T = \frac{A_T^{\lambda}\rho_w(\lambda)}{(1-\rho_w(\lambda)/C^{\lambda})} \quad (1)$$

where $\rho_w(\lambda)$ is water reflectance at wavelength λ, A_T and C are wavelength-depend calibration coefficients. The red band (645 nm) band is used when $\rho_w(645) < 0.05$, and the NIR band (859 nm) is used when $\rho_w(645) > 0.07$. A linear weighing function, of which the weight of the algorithm (w) changes linearly from 0 at $\rho_w(645) = 0.05$ to 1 at $\rho_w(645) = 0.07$, is used when $0.05 < \rho_w(645) < 0.07$ to assure a smooth transition, according to the equation below:

$$T = (1 - w) \cdot T_{645} + w \cdot T_{859} \quad (2)$$

The original algorithm was developed based on the Moderate Resolution Imaging

Spectroradiometer (MODIS). The wavelengths red band and NIR band were adjusted to 664 nm for red and 842 nm for NIR since we are using Sentinel-2.

Considering the water dynamic nature, the mean turbidity from a 5×5 pixel window of each station was extracted by Python. The minimum, lower quartile, mean, median, upper quartile, and maximum values for each square were also calculated.

3.2 Ground based measurement

3.2.1 *In situ* Light Transmission

Monitoring of LA coastal water is carried out by the LA Sanitation's Environmental Monitoring Division to determine if Ocean Plan and Basin Plan objectives for physical and chemical parameters and bacteria are being met. The water samples were collected on a quarterly basis from 54 offshore stations locating from the nearshore to approximately 10 kilometers offshore, covering the Los Angeles coastline.

The *in situ* light transmission measurements are provided by LA sanitation from the 54 stations around the Santa Monica Bay area. Samples were collected from 2018-2019 and were analyzed using the analytical methods described in 40 CFR § 136 (*ORDER R4-2017-XXXX NPDES NO. CA0109991*, 2017).

3.2.2 Other *in situ* measurements

Beach water was sampled (2 liters) about 50 cm beneath the sea surface from 2021 summer to 2021 fall.

Total coliforms (TC), *E. coli* (EC), and enterococci (ENT) were assessed using the IDEXX® (https://www.idexx.com/) chromogenic substrate (CS) method according to

the manufacturer's instructions. Colilert-18 media were used for enumeration of TC and EC, while Enterolert media were used for ENT. Samples were diluted to 1:10 in MilliQ water considering the coastal water quality. The FIB results were quantified using the most probable number (MPN) method by counting the positive wells in a 96-well IDEXX Quanti-Tray.

TSS was determined gravimetrically according to the standard guidelines (*2540 SOLIDS*, 2018) by weighing the dried residues after membrane filtration (glass microfiber, particle retention 1.5 µm, 47 mm diameter).

Spectrophotometric analysis was done by the LAMBDA 365 UV/Vis Spectrophotometer from PerkinElmer (https://www.perkinelmer.com/). A spectral scan focusing on absorption of light was carried out between 190 nm to 1100 nm. The spectrophotometer was set to baseline subtraction to account for absorption by blanks (MilliQ water samples), after which absorption spectra for respective coastal water samples were taken and subtracted from final absorbance measurements.

4. Results

4.1 Sentinel-2 Data vs. *in Situ* Light transmission

The results of the *in situ* light transmission and Sentinel-2 derived turbidity (in FNU) values are compared and the linear regression between the two variables is shown below. The light transmission and turbidity generally show a negative trend (Figure 2(a)). The turbidity decreases while the *in situ* light transmission increasing. This result is same as previous studies (J. C. McCarthy et al., 1974; Telesnicki & Goldberg, 1995). Figure 2(b) shows a strong negative correlation between the Sentinel-2 derived turbidity and *in situ* light transmission (r^2=0.6702, Pearson's r =-0.82).

Figure 2. (a) Comparison between the *in situ* light transmission and corresponding satellite-derived turbidity from 2018-2019. (b) Linear regression analysis of satellite-derived turbidity on percent light transmission from 2018-2019.

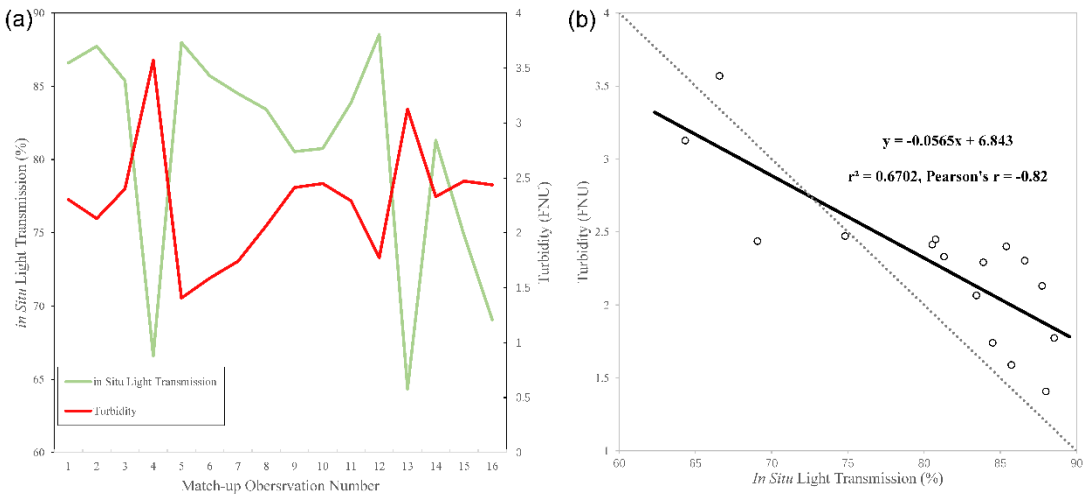

4.2 Comparison of Sentinel-2 Data vs. *in Situ* and Laboratory Data Results

To better correspond with the Dogliotti et al. (2015) algorithm, we chose the same wavelengths (665 nm and 842 nm) to compare the correlation between *in situ*

absorbance data and satellite-derived satellite data. The spectra curves of the coastal waters were obviously different in shape from those of the ocean water bodies from our results. Figure 3(a) are linear graphs establishing the positive relationship between absorbance at both wavelengths and Sentinel-2 derived turbidity. As can be seen from the graph, the absorbance at red band was higher than that at NIR band. The results of the correlational analysis are compared in Figure 3(b). It is worth noting that the absorbance at 665 nm shows a better correlation (r^2=0.6387, Pearson's r=0.799) with the ACOLITE-derived turbidity data compared to the absorbance at 842 nm (r^2=0.6361, Pearson's r=0.798), although the difference is not significant of the Pearson's correlation coefficient.

Figure 3. (a)Comparison between the *in situ* Absorbance and corresponding satellite-derived turbidity from 2021 summer - fall. (b) Linear regression analysis of *in situ* Absorbance on satellite-derived turbidity from 2021 summer - fall.

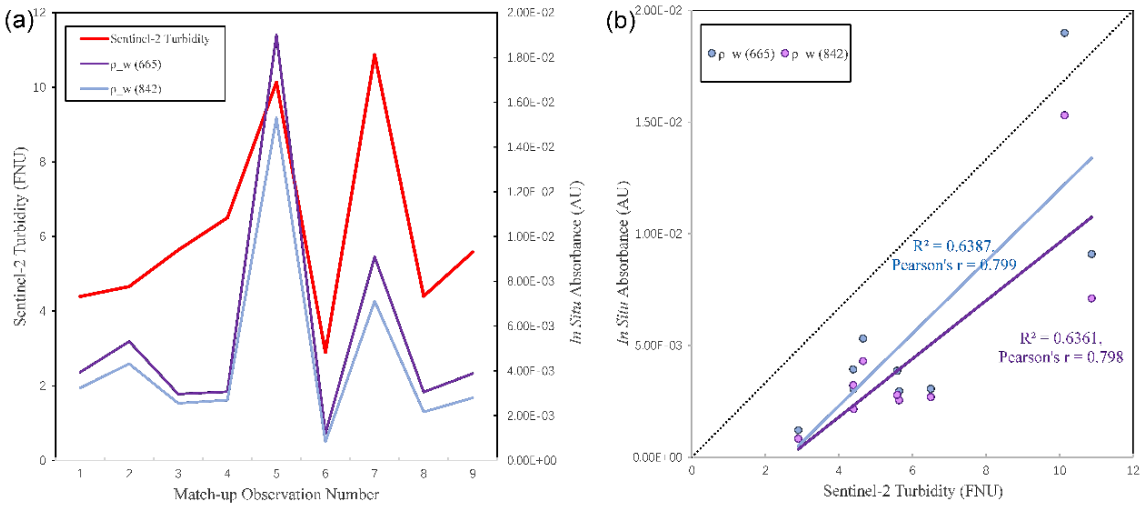

Table 3 illustrates the intercorrelations among the measurements of water quality from *in situ* samples and remote sensing-derived data. Significance levels for every correlation were calculated. Data from this table could be compared with the data in Figure 3.

Table 3. Pearson's correlation coefficients for all tested *in situ* parameters and Sentinel-2 turbidity. Moderate correlations are highlighted in yellow.

Parameters	ACOLITE	$\rho_w(665)$	$\rho_w(842)$	TSS	TC	EC	ENT
ACOLITE	1						
$\rho_w(665)$	0.799	1					
$\rho_w(842)$	0.798	0.999	1				
TSS	0.641	0.450	0.466	1			
TC	-0.008	-0.187	-0.168	0.501	1		
EC	-0.058	-0.188	-0.169	0.464	0.996	1	
ENT	0.141	0.003	0.021	0.582	0.980	0.977	1

This set of data shows the high correlation between satellite data and *in situ* observations. A good consistency existed between the remote sensing derived turbidity and *in situ* TSS (Pearson's r = 0.641), which is consistent with our inference. Positive correlations are also found between TSS and FIB, of which r=0.501, 0.464, and 0.582 for total coliform, *E. coli* and enterococci, respectively. ENT shows the best correlation compared with other two fecal bacteria indicators. TC and EC have a relatively similar linear relationship with TSS, while ENT have a better linear relationship but with a linear equation different from other two indicators (Figure 4). No significant correlation was found between satellite-derived turbidity and fecal indicator bacteria.

Figure 4. Linear regression analysis for MPN of the *in situ* FIB vs. *in situ* TSS.

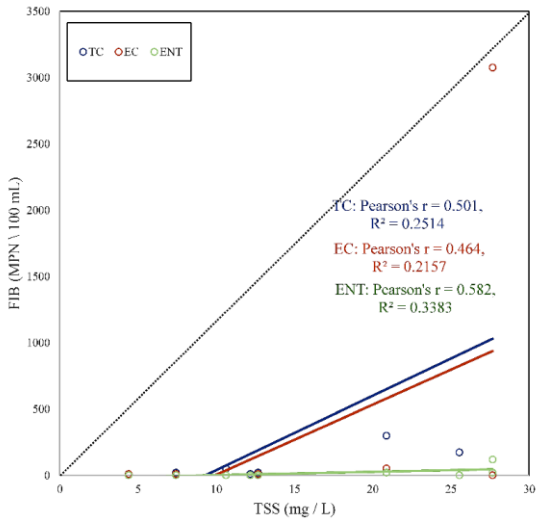

5. Discussion

The main purpose of this study was to investigate the ability of high spatial resolution satellite data for estimating water quality. Many studies have been done on to validate the correlation between *in situ* water quality and remote-sensing water quality data using the high-resolution satellite. The possibility of using Sentinel-2 products to monitor coastal water quality around the Santa Monica Bay, Los Angeles, California was examined in this study. We collected field data between 22nd July and 26th October 2021 on the Sentinel- 2A/B passing days to ensure the consistency. *In situ* water quality variables used in this research included light transmission, TC, *E. coli*, *Enterococcus*, light absorbance, and TSS, and regression analysis was used to investigate the relations between the turbidity derived by Sentinel-2 reflectance data and the filed water quality data. Several studies have presented the possibility of determining water quality with remote sensing imaginary, especially Landsat-8 (with a spatial resolution of 30 meters) (Quang et al., 2017; Trinh et al., 2017; Luis et al., 2019). Besides, most of the research are focused on inland water bodies (e.g., lakes or rivers) (Güttler et al., 2013; Guo et al., 2017; Garg et al., 2020; Zhou et al., 2021). Thus, focusing on coastal water around southern California, we evaluate the ability of Sentinel-2 for monitoring water quality. To our knowledge, only a few studies can be found in the literature exploring the correlation of *in situ* optical water characteristics with remote sensing data.

The main results of the study showed a significant relation between the *in situ* optical parameters of water quality and Sentinel-2 turbidity. Aiming at validating

whether Sentinel-2 could be used to monitor coastal water quality around Los Angeles, we first analyzed the existing field data (light transmission) from 2018 to 2019 provided by LA Sanitation to compare with the satellite derived turbidity. A high negative correlation coefficient (Pearson's r = -0.82, $p<0.001$) was found. There are studies claiming that turbidity could be surrogated by the transmitted light intensity with a negative correlation, due to the greatest ability of scattering centers in the water sample scattering the incident light (Sefa-Ntiri et al., 2014; Telesnicki & Goldberg, 1995). Our results show the same relationship according to current data.

To further verify the results, we collected coastal water samples from summer 2021 to fall 2021, and specifically focused on the water quality indicator, which is optically active, absorbance in this case. From the Beer–Lambert Law, absorbance is negatively correlated with light transmission (Mäntele & Deniz, 2017):

$$A = -log\ T = log\ \frac{I_0}{I} \tag{3}$$

where A is absorbance, T is transmission, I_0 and I are intensity of the measuring beam before/after passing through the sample, respectively. Thus, we can conjecture that the higher the turbidity is, the higher the absorbance will be. From our result in Figure 2 and the Beer-Lambert Law, the *in situ* absorbance is supposed to show a positive relationship with turbidity derived by Sentinel-2. And according to Figure 3, the correlation coefficients for both wavelengths are positive (Pearson's r = 0.799 and 0.798, respectively), indicating that our assumption is right. The Pearson's r value of $\rho_w(665)$ has a higher correlation compared with $\rho_w(842)$, indicating that compared with NIR bands, red bands are more sensitive towards turbidity estimation.

This is similar with the previous research, which presented that the red bands works better for low turbidity levels monitoring (Z. Chen et al., 2007; Bustamante et al., 2009; Chawla et al., 2020).

We also conducted experiments on other water quality indicators, including FIB and TSS. The monitoring of total suspended sediments is critical for analyzing river dynamics as it serves as an indicator for water quality and used in sediment discharge and transport applications (Petersen et al., 2017). As a parameter directly affected by suspended particles concentration in water, turbidity is often used as a proxy of sediment concentration in the water body (Rügner et al., 2013). The relationship between turbidity and TSS depends on the size, density, shape and type of the suspended particles in general, as well as watercolor. Ideally, the TSS, absorbance and satellite derived turbidity should all have a positive correlation with each other. FIB, generally using as an indicator of fecal pollution in water samples, is a significant water quality parameter directly affected human health (LeClerc et al., 1996).

The summary statistics for the comparison of *in situ* water quality parameters we tested in this study are shown in Table 3. As we can see, TSS have a positive correlation with red and NIR band absorbance, all three types of FIB. The result is consistent with our assumptions, and also can be seen as a proof that our *in situ* parameters concentrations are reliable. Nevertheless, TC and EC were less correlated with *in situ* TSS than ENT, which may be because ENT is more likely to attach to particles (Soupir et al., 2010). It is noticeable that the FIB is always higher for Santa Monica beach than other sampling beach sites, which may be due to its high passenger flow as a tourist

attraction. In addition, the food tourists leaving on the beach also attract numbers of birds, also inducing an increase in the FIB because of the bird fecal.

This research provides a validation of the accuracy of satellite derived turbidity value compared to the *in situ* measurements in the Santa Monica Bay area, exhibiting the promising capability of Sentinel-2 to support coastal management as a valuable tool for turbidity monitoring. Besides, the study also demonstrates that the optical properties of in situ water samples could be used as a validation of satellite-derived turbidity data. Nonetheless, additional insights must be considered for inspection of a wider range of turbidity concentrations and other water quality parameters (chlorophyll-a, Colored Dissolved Organic Matter, etc.) to establish a continuous framework for the ongoing services relying on both Sentinel-2 twin satellites. In general, Sentinel-2 data can be used to help with water quality monitoring in coastal areas. However, the disadvantage is that satellites are susceptible to weather and turbidity is also relatively susceptible to sand in coastal water.

It is well documented that remote sensing may offer preliminary qualitative estimates of coastal water quality; however, it is necessary to establish the relationship between remotely sensed turbidity values and those observed using samples collected at the site of the interest, in this case, the Santa Monica Bay. Research focusing on high turbidity coastal areas is also needed, since the research reported here is addressing a relatively low turbidity area.

Reference

2540 SOLIDS. (2018). https://doi.org/10.2105/SMWW.2882.030

Akbar, T. A., Hassan, Q. K., & Achari, G. (2010). *A REMOTE SENSING BASED FRAMEWORK FOR PREDICTING WATER QUALITY OF DIFFERENT SOURCE WATERS*. *34*, 1–4.

Bilotta, G. S., & Brazier, R. E. (2008). Understanding the influence of suspended solids on water quality and aquatic biota. *Water Research*, *42*(12), 2849–2861. https://doi.org/10.1016/j.watres.2008.03.018

Bray, N. A., Keyes, A., & Morawitz, W. M. L. (1999). The California Current system in the Southern California Bight and the Santa Barbara Channel. *Journal of Geophysical Research: Oceans*, *104*(C4), 7695–7714. https://doi.org/10.1029/1998JC900038

Bustamante, J., Pacios, F., Díaz-Delgado, R., & Aragonés, D. (2009). Predictive models of turbidity and water depth in the Doñana marshes using Landsat TM and ETM+ images. *Journal of Environmental Management*, *90*(7), 2219–2225. https://doi.org/10.1016/j.jenvman.2007.08.021

Büttner, Gy., Korándi, M., Gyömörei, A., Köte, Zs., & Szabó, Gy. (1987). Satellite remote sensing of inland waters: Lake Balaton and reservoir Kisköre. *Acta Astronautica*, *15*(6–7), 305–311. https://doi.org/10.1016/0094-5765(87)90165-2

CALIFORNIA: 2020 Census. (2021). U.S. Census Bureau, 2020. https://www.census.gov/library/stories/state-by-state/california-population-

change-between-census-decade.html

Cao, C., Xiong, J., Blonski, S., Liu, Q., Uprety, S., Shao, X., Bai, Y., & Weng, F. (2013). Suomi NPP VIIRS sensor data record verification, validation, and long-term performance monitoring: VIIRS SDR CAL/VAL AND PERFORMANCE. *Journal of Geophysical Research: Atmospheres*, *118*(20), 11,664-11,678. https://doi.org/10.1002/2013JD020418

Chawla, I., Karthikeyan, L., & Mishra, A. K. (2020). A review of remote sensing applications for water security: Quantity, quality, and extremes. *Journal of Hydrology*, *585*, 124826. https://doi.org/10.1016/j.jhydrol.2020.124826

Chen, S., Huang, W., Chen, W., & Chen, X. (2011). An enhanced MODIS remote sensing model for detecting rainfall effects on sediment plume in the coastal waters of Apalachicola Bay. *Marine Environmental Research*, *72*(5), 265–272. https://doi.org/10.1016/j.marenvres.2011.09.014

Chen, Z., Muller-Karger, F. E., & Hu, C. (2007). Remote sensing of water clarity in Tampa Bay. *Remote Sensing of Environment*, *109*(2), 249–259. https://doi.org/10.1016/j.rse.2007.01.002

Climate of Los Angeles, California (NOAA Technical Memorandum NESS). (2000). Washington: U.S. Dept. of Commerce, National Oceanic and Atmospheric Administration, National Environmental Satellite Service.

Cloern, J. E. (1987). Turbidity as a control on phytoplankton biomass and productivity in estuaries. *Continental Shelf Research*, *7*(11–12), 1367–1381. https://doi.org/10.1016/0278-4343(87)90042-2

Dogliotti, A. I., Ruddick, K. G., Nechad, B., Doxaran, D., & Knaeps, E. (2015). A single algorithm to retrieve turbidity from remotely-sensed data in all coastal and estuarine waters. *Remote Sensing of Environment*, *156*, 157–168. https://doi.org/10.1016/j.rse.2014.09.020

Donlon, C. J., & Robinson, I. S. (1998). Radiometric Validation of *ERS-1* Along-Track Scanning Radiometer Average Sea Surface Temperature in the Atlantic Ocean. *Journal of Atmospheric and Oceanic Technology*, *15*(3), 647–660. https://doi.org/10.1175/1520-0426(1998)015<0647:RVOEAT>2.0.CO;2

Flores-Anderson, A. I., Griffin, R., Dix, M., Romero-Oliva, C. S., Ochaeta, G., Skinner-Alvarado, J., Ramirez Moran, M. V., Hernandez, B., Cherrington, E., Page, B., & Barreno, F. (2020). Hyperspectral Satellite Remote Sensing of Water Quality in Lake Atitlán, Guatemala. *Frontiers in Environmental Science*, *8*, 7. https://doi.org/10.3389/fenvs.2020.00007

Garg, V., Aggarwal, S. P., & Chauhan, P. (2020). Changes in turbidity along Ganga River using Sentinel-2 satellite data during lockdown associated with COVID-19. *Geomatics, Natural Hazards and Risk*, *11*(1), 1175–1195. https://doi.org/10.1080/19475705.2020.1782482

Gierach, M. M., Holt, B., Trinh, R., Jack Pan, B., & Rains, C. (2017). Satellite detection of wastewater diversion plumes in Southern California. *Estuarine, Coastal and Shelf Science*, *186*, 171–182. https://doi.org/10.1016/j.ecss.2016.10.012

Ginger, L., Lucy, R., Shelley, L., Katherine, P., Talia, W., & Gabriele, M. (2021). *2021-2021 Beach Report Card*. Heal the Bay. https://healthebay.org/wp-

content/uploads/2021/06/Beach-Report-Card-2020-2021.pdf

Glasgow, H. B., Burkholder, J. M., Reed, R. E., Lewitus, A. J., & Kleinman, J. E. (2004). Real-time remote monitoring of water quality: A review of current applications, and advancements in sensor, telemetry, and computing technologies. *Journal of Experimental Marine Biology and Ecology*, *300*(1–2), 409–448. https://doi.org/10.1016/j.jembe.2004.02.022

González-Márquez, L. C., Torres-Bejarano, F. M., Rodríguez-Cuevas, C., Torregroza-Espinosa, A. C., & Sandoval-Romero, J. A. (2018). Estimation of water quality parameters using Landsat 8 images: Application to Playa Colorada Bay, Sinaloa, Mexico. *Applied Geomatics*, *10*(2), 147–158. https://doi.org/10.1007/s12518-018-0211-9

Gordon, H. R., Clark, D. K., Mueller, J. L., & Hovis, W. A. (1980). Phytoplankton Pigments from the Nimbus-7 Coastal Zone Color Scanner: Comparisons with Surface Measurements. *Science*, *210*(4465), 63–66. https://doi.org/10.1126/science.210.4465.63

Guo, K., Zou, T., Jiang, D., Tang, C., & Zhang, H. (2017). Variability of Yellow River turbid plume detected with satellite remote sensing during water-sediment regulation. *Continental Shelf Research*, *135*, 74–85. https://doi.org/10.1016/j.csr.2017.01.017

Güttler, F. N., Niculescu, S., & Gohin, F. (2013). Turbidity retrieval and monitoring of Danube Delta waters using multi-sensor optical remote sensing data: An integrated view from the delta plain lakes to the western–northwestern Black

Sea coastal zone. *Remote Sensing of Environment*, *132*, 86–101. https://doi.org/10.1016/j.rse.2013.01.009

Hellweger, F. L., Schlosser, P., Lall, U., & Weissel, J. K. (2004). Use of satellite imagery for water quality studies in New York Harbor. *Estuarine, Coastal and Shelf Science*, *61*(3), 437–448. https://doi.org/10.1016/j.ecss.2004.06.019

Hoge, F. E., Williams, M. E., Swift, R. N., Yungel, J. K., & Vodacek, A. (1995). Satellite retrieval of the absorption coefficient of chromophoric dissolved organic matter in continental margins. *Journal of Geophysical Research*, *100*(C12), 24847. https://doi.org/10.1029/95JC02561

Hovis, W. A., Clark, D. K., Anderson, F., Austin, R. W., Wilson, W. H., Baker, E. T., Ball, D., Gordon, H. R., Mueller, J. L., El-Sayed, S. Z., Sturm, B., Wrigley, R. C., & Yentsch, C. S. (1980). Nimbus-7 Coastal Zone Color Scanner: System Description and Initial Imagery. *Science*, *210*(4465), 60–63. https://doi.org/10.1126/science.210.4465.60

Kahru, M., & Mitchell, B. G. (2001). Seasonal and nonseasonal variability of satellite-derived chlorophyll and colored dissolved organic matter concentration in the California Current. *Journal of Geophysical Research: Oceans*, *106*(C2), 2517–2529. https://doi.org/10.1029/1999JC000094

Kutser, T., Pierson, D. C., Kallio, K. Y., Reinart, A., & Sobek, S. (2005). Mapping lake CDOM by satellite remote sensing. *Remote Sensing of Environment*, *94*(4), 535–540. https://doi.org/10.1016/j.rse.2004.11.009

LeClerc, J. E., Li, B., Payne, W. L., & Cebula, T. A. (1996). High Mutation Frequencies

Among *Escherichia coli* and *Salmonella* Pathogens. *Science*, *274*(5290), 1208–1211. https://doi.org/10.1126/science.274.5290.1208

Luis, K. M. A., Rheuban, J. E., Kavanaugh, M. T., Glover, D. M., Wei, J., Lee, Z., & Doney, S. C. (2019). Capturing coastal water clarity variability with Landsat 8. *Marine Pollution Bulletin*, *145*, 96–104. https://doi.org/10.1016/j.marpolbul.2019.04.078

Mäntele, W., & Deniz, E. (2017). UV–VIS absorption spectroscopy: Lambert-Beer reloaded. *Spectrochimica Acta Part A: Molecular and Biomolecular Spectroscopy*, *173*, 965–968. https://doi.org/10.1016/j.saa.2016.09.037

McCarthy, J. C., Pyle, T. E., & Griffin, G. M. (1974). Light transmissivity, suspended sediments and the legal definition of turbidity. *Estuarine and Coastal Marine Science*, *2*(3), 291–299. https://doi.org/10.1016/0302-3524(74)90019-X

McCarthy, M. J., Colna, K. E., El-Mezayen, M. M., Laureano-Rosario, A. E., Méndez-Lázaro, P., Otis, D. B., Toro-Farmer, G., Vega-Rodriguez, M., & Muller-Karger, F. E. (2017). Satellite Remote Sensing for Coastal Management: A Review of Successful Applications. *Environmental Management*, *60*(2), 323–339. https://doi.org/10.1007/s00267-017-0880-x

Nazeer, M., & Nichol, J. E. (2016). Development and application of a remote sensing-based Chlorophyll-a concentration prediction model for complex coastal waters of Hong Kong. *Journal of Hydrology*, *532*, 80–89. https://doi.org/10.1016/j.jhydrol.2015.11.037

Nezlin, N. P., DiGiacomo, P. M., Jones, B. H., Reifel, K. M., Warrick, J. A., Johnson,

S. C., & Mengel, M. J. (2007). *MODIS imagery as a tool for synoptic water quality assessments in the southern California coastal ocean* (R. J. Frouin, Ed.; p. 66800T). https://doi.org/10.1117/12.732754

ORDER R4-2017-XXXX NPDES NO. CA0109991 (WASTE DISCHARGE REQUIREMENTS AND NATIONAL POLLUTANT DISCHARGE ELIMINATION SYSTEM PERMIT FOR THE CITY OF LOS ANGELES, HYPERION TREATMENT PLANT DISCHARGE TO THE PACIFIC OCEAN). (2017). U.S. ENVIRONMENTAL PROTECTION AGENCY.

Ouellette, W., & Getinet, W. (2016). Remote sensing for Marine Spatial Planning and Integrated Coastal Areas Management: Achievements, challenges, opportunities and future prospects. *Remote Sensing Applications: Society and Environment*, *4*, 138–157. https://doi.org/10.1016/j.rsase.2016.07.003

Peel, M. C., Finlayson, B. L., & McMahon, T. A. (2007). Updated world map of the Köppen-Geiger climate classification. *Hydrology and Earth System Sciences*, *11*(5), 1633–1644. https://doi.org/10.5194/hess-11-1633-2007

Petersen, C., Jovanovic, N., Le Maitre, D., & Grenfell, M. (2017). Effects of land use change on streamflow and stream water quality of a coastal catchment. *Water SA*, *43*(1), 139. https://doi.org/10.4314/wsa.v43i1.16

Quang, N., Sasaki, J., Higa, H., & Huan, N. (2017). Spatiotemporal Variation of Turbidity Based on Landsat 8 OLI in Cam Ranh Bay and Thuy Trieu Lagoon, Vietnam. *Water*, *9*(8), 570. https://doi.org/10.3390/w9080570

Ritchie, J. C. (1976). Remote Sensing of Suspended Sediments in Surface Waters.

PHOTOGRAMMETRIC ENGINEERING, 7.

Rügner, H., Schwientek, M., Beckingham, B., Kuch, B., & Grathwohl, P. (2013). Turbidity as a proxy for total suspended solids (TSS) and particle facilitated pollutant transport in catchments. *Environmental Earth Sciences*, *69*(2), 373–380. https://doi.org/10.1007/s12665-013-2307-1

Sebastiá-Frasquet, M.-T., Aguilar-Maldonado, J. A., Santamaría-Del-Ángel, E., & Estornell, J. (2019). Sentinel 2 Analysis of Turbidity Patterns in a Coastal Lagoon. *Remote Sensing*, *11*(24), 2926. https://doi.org/10.3390/rs11242926

Sefa-Ntiri, B., Kwakye-Awuah, B., & Williams, C. (2014). EFFECT OF ZEOLITE TYPES LTX AND LTA ON PHYSICOCHEMICAL PARAMETERS OF DRINKING WATER SAMPLES IN GHANA, ASSISTED BY LIGHT TRANSMISSION EXPERIMENT. *International Journal of Research in Engineering and Technology*, *03*(03), 686–692. https://doi.org/10.15623/ijret.2014.0303126

Shanmugam, P., He, X., Singh, R. K., & Varunan, T. (2018). A modern robust approach to remotely estimate chlorophyll in coastal and inland zones. *Advances in Space Research*, *61*(10), 2491–2509. https://doi.org/10.1016/j.asr.2018.02.024

Soupir, M. L., Mostaghimi, S., & Dillaha, T. (2010). Attachment of *Escherichia coli* and Enterococci to Particles in Runoff. *Journal of Environmental Quality*, *39*(3), 1019–1027. https://doi.org/10.2134/jeq2009.0296

Sugumaran, R. (2007). Monitoring intra-annual water quality variations using airborne hyperspectral remote sensing data in Iowa lakes. *Journal of Applied Remote*

Sensing, *1*(1), 013533. https://doi.org/10.1117/1.2790445

Telesnicki, G. J., & Goldberg, W. M. (1995). Comparison of Turbidity Measurement by Nephelometry and Transmissometry and its Relevance to Water Quality Standards. *BULLETIN OF MARINE SCIENCE*, *57*, 8.

Trinh, R. C., Fichot, C. G., Gierach, M. M., Holt, B., Malakar, N. K., Hulley, G., & Smith, J. (2017). Application of Landsat 8 for Monitoring Impacts of Wastewater Discharge on Coastal Water Quality. *Frontiers in Marine Science*, *4*, 329. https://doi.org/10.3389/fmars.2017.00329

Vanhellemont, Q. (2019). Adaptation of the dark spectrum fitting atmospheric correction for aquatic applications of the Landsat and Sentinel-2 archives. *Remote Sensing of Environment*, *225*, 175–192. https://doi.org/10.1016/j.rse.2019.03.010

Vanhellemont, Q. (2020). Sensitivity analysis of the dark spectrum fitting atmospheric correction for metre- and decametre-scale satellite imagery using autonomous hyperspectral radiometry. *Optics Express*, *28*(20), 29948. https://doi.org/10.1364/OE.397456

Vanhellemont, Q., & Ruddick, K. (2014). Turbid wakes associated with offshore wind turbines observed with Landsat 8. *Remote Sensing of Environment*, *145*, 105–115. https://doi.org/10.1016/j.rse.2014.01.009

Vanhellemont, Q., & Ruddick, K. (2015). Advantages of high quality SWIR bands for ocean colour processing: Examples from Landsat-8. *Remote Sensing of Environment*, *161*, 89–106. https://doi.org/10.1016/j.rse.2015.02.007

Vanhellemont, Q., & Ruddick, K. (2016). *ACOLITE FOR SENTINEL-2: AQUATIC APPLICATIONS OF MSI IMAGERY*. 8.

Vanhellemont, Q., & Ruddick, K. (2018). Atmospheric correction of metre-scale optical satellite data for inland and coastal water applications. *Remote Sensing of Environment*, *216*, 586–597. https://doi.org/10.1016/j.rse.2018.07.015

Zhou, Q., Wang, J., Tian, L., Feng, L., Li, J., & Xing, Q. (2021). Remotely sensed water turbidity dynamics and its potential driving factors in Wuhan, an urbanizing city of China. *Journal of Hydrology*, *593*, 125893. https://doi.org/10.1016/j.jhydrol.2020.125893